Photonic Transitions (1.4 eV–2.8 eV) in Silicon p^+np^+ Injection-Avalanche CMOS LEDs as Function of Depletion Layer Profiling and Defect Engineering

Lukas Willem Snyman, *Member, IEEE*, Monuko du Plessis, *Senior Member, IEEE*, and Enrico Bellotti

***Abstract*—p^+np^+ CMOS Si LED structures were modeled in order to investigate the effect of various depletion layer profiles and defect engineering on the photonic transitions in the 1.4–2.8 eV, 450–750 nm regime. Modeling shows that by utilizing a short linear increasing E-field in the p^+n reverse-biased junction with a gradient of approximately 5×10^5 V cm^{-1}. μm^{-1}, and injecting carriers from an adjacent p^+n junction, increased localized optical yield by a factor 50–100. A number of device designs were realized using CMOS 0.35 μm technology. The device design involves normal CMOS design and processing procedures with no excessive microdimensioning. The current devices operated in the 6–8 V, 1 μA–2 mA regime, and yield emission intensities of up to 100 nW μm^{-2}. The current emission levels are about three orders higher than the low-frequency detectability limit of Si CMOS p-n detectors of corresponding area, which make diverse electro-optical applications such as MOEMS devices, and diverse optical signal processing and wave-guiding and the development of "smart chips" feasible in standard CMOS integrated circuitry.**

***Index Terms*—CMOS integrated circuitry, electroluminescence, light-emitting diodes (LEDs), physical modeling, silicon, silicon photonics.**

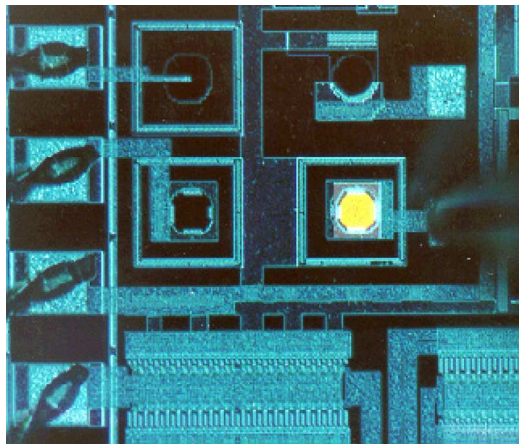

Fig. 1. The 60-μm diameter Si avalanche-based LED and optical interface as realized in 1.2-μm Si CMOS technology with no alterations to the design and processing procedures.

I. Introduction

VARIOUS researchers [1]–[5] have highlighted the need for small-dimension, efficient light emitters which are compatible with mainstream silicon CMOS integrated circuit technology. The realization of sufficiently efficient light emitters are currently a major technological challenge and will considerably boost opto-electronic applications and integration at the integrated circuit level. Although longer wavelength light emitters have application in integrating data-telecommunication systems on the chip level, shorter wavelength Si light emitters can find wide-scale applications as on chip opto-couplers, short-range wave-guiding-based systems, and on-chip mechanical-optical sensor (MOEMS) applications [6]. Wada *et al.* [7] have proposed the utilization of 450-nm-based LEDs for clock-pulsing in large diameter, next-generation silicon microprocessor circuits. The main advantages of the avalanche Si LED technology are its ease of integration into standard CMOS technology with no variation to design and processing procedures as well as its very high modulation speed possibilities (>10 GHz) [8].

Light emission from silicon devices has been realized in reverse-biased p-n avalanche structures [9]–[14]. Various theories have been put forward in order to explain the phenomenon. These include phonon-assisted intraband relaxation phenomena [14], [15], as well as phonon interband recombination processes [15]. In-depth theoretical modeling and experimental evidence indicated that the dominant photonic generation processes may be from intraband phonon-assisted relaxation processes, mainly in the conduction band [11].

However, this technology seemed not very viable because of the low external power and quantum conversion efficiencies which were reported for the early devices (10^{-8} to 10^{-7}) [12].

Snyman, du Plessis, and Aharoni have over some time realized a series of *practical* and *utilizable* light-emitting devices (Si LEDs) in *standard CMOS* technology using the avalanche light-emitting phenomenon (see Fig. 1) [16]–[25]. This was mainly achieved by using novel surface engineering, current density modeling and dynamic carrier density engineering techniques. The developed devices showed about three orders of increase

Manuscript received June 24, 2009; revised October 01, 2009. Current version published March 10, 2010. This work was supported by the National Research Foundation in South Africa. Some of the content in this paper forms the subject of USA Patent 6,111,271 of August 29, 2000, USA Patent 5,944,720 of November 20, 1999, SA Patent Application 2008/00593 of January 21, 2008, and a PCT Patent Application IB2009/050209 of 2009-01-30.

L. W. Snyman is at the Laboratory for Innovative Electronic Systems, Department of Electrical Engineering, Tshwane University of Technology (TUT), Pretoria 0001, South Africa (e-mail: snymanlw@tut.ac.za).

M. du Plessis is with the Carl and Emily Fuchs Institute of Micro-electronics, University of Pretoria, Pretoria 0002, South Africa (e-mail: monuko.du.plessis@up.ac.za).

E. Bellotti is with the Department of Electrical and Computer Engineering, Boston University, Boston, MA U02115 USA (e-mail: bellotti@bu.edu).

Color versions of one or more of the figures in this paper are available online at http://ieeexplore.ieee.org.

Digital Object Identifier 10.1109/JQE.2009.2036746

in optical output as compared with previous similar work [21], [25]. Particularly promising results have recently been obtained regarding further increasing the efficiency, as well as the emitted intensity with what we call the InSiAva (Injection-enhanced Silicon in Avalanche) technology [26], [27]. This technology utilizes the hypothesis that the light emission in these structures can be increased due to interaction of high-energy (hot) electrons, as excited in the avalanching junction, with low-energy (cool) energy holes injected into the avalanching junction by a nearby forward-biased pn junction.

In this paper, we report on advances made with regard to understanding the mechanisms involved with light emission from p^+np^+ injection-avalanche structures, as well as with regard to progresses made with increasing the electrical-to-optical conversion efficiencies as associated with these structures. Specifically, we introduce dedicated modeling, depletion layer profiling, and defect engineering investigation techniques. We also make important derivations with regard to the internal optical yield as derived from these devices.

II. Stimulating Higher Than Bandgap Optical Transitions in Silicon

Fig. 2 illustrates some of the conceptual design aspects of our p^+np^+ injection-avalanche technology, referring to specific device zones, electric field distribution, and possible photonic transitions in the silicon energy bandgap. Fig. 2(a) shows the main three operating regions of the device: a high field excitation zone generating energetic carriers, a relaxation and recombination zone for excited electrons as they traverse the depletion region of the first junction and a so-called injection zone where low-energy carriers is injected into the depletion region of the first junction by forward-biased second junction. The following section describes more in detail the device operation.

1) Upon reverse voltage biasing the device, a high linearly increasing electric field is created with its maximum at the one p^+n interface [Fig. 2(b)]. At some bias voltage, the E-field at the interface region attains high enough values such that charge multiplication (avalanche) processes occur in a narrow zone surrounding the interface. Energetic ("hot") electrons are transferred toward the n-side of the junction and energetic holes are transferred toward the p^+ side of the junction.
2) Since the E-field decays linearly with distance away from the p^+n interface [Fig. 2(b)], the transferred electrons soon reach regions where the E-field is not high enough to sustain impact ionization and consequently carrier multiplication, and they are transferred away from the junction in the linearly decreasing E-field. This region is referred to the depletion zone or drift zone of the device.
3) If a second np^+ junction is placed near the depletion or drift zone [Fig. 2(b)], and this junction is forward-biased, low-energy holes may be injected into the drift zone. They will drift in a opposite direction and interact with the excited energetic electrons as well as with defect centers in the depletion region.

   Early investigations into the origin of light emission processes in avalanching np silicon junction suggested that the main light production processes are related to host silicon atom ionization processes in the high field avalanching conditions, followed by subsequent intraband relaxation processes and phonon-assisted indirect band-to-band transitions [10], [11], [15].
4) In the light-emitting structure presented in this work, some high-energy interband optical transitions in the silicon band structure are exploited by utilizing the recombination behavior between excited carriers and lower energy carriers, and by utilizing some novel device designs. Fig. 2(c)

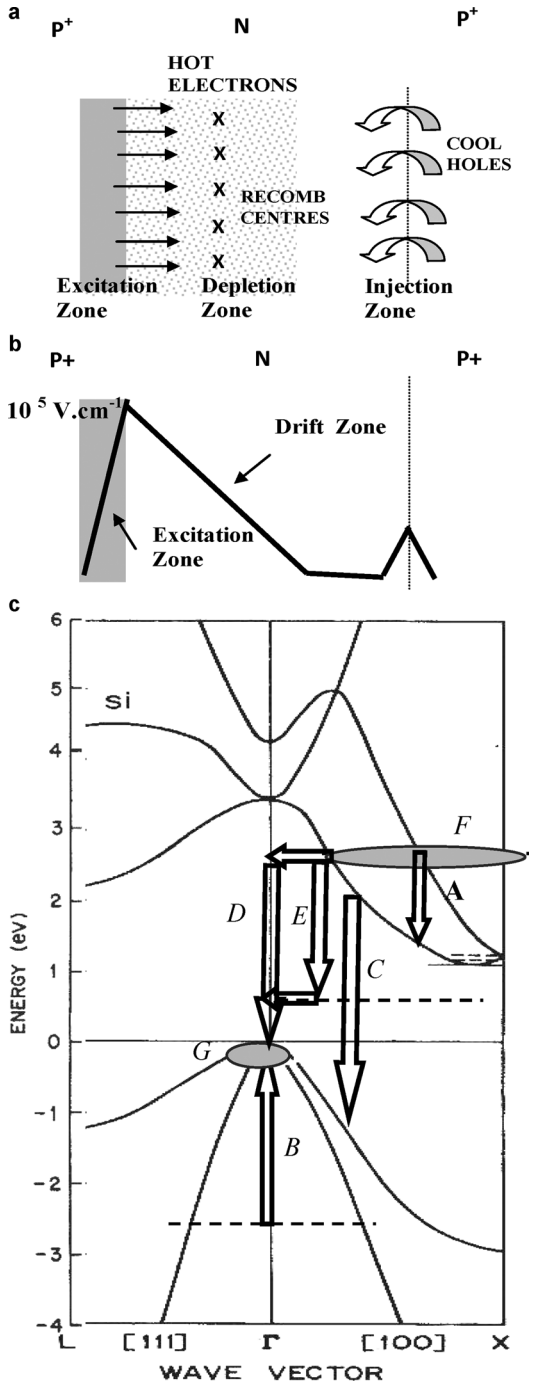

Fig. 2. Schematic representations of the design concepts for a p^+np^+ injection-avalanche CMOS Si LED. (a) Structure of the device. (b) Electric field profile through the device. (c) Possible photonic energy transitions for the device in the Si band diagram.

demonstrates some of the photonic transition processes that may be stimulated in the above scenario. During the avalanche process the carriers are accelerated in the high electric field region of the depletion layer but lose most of their energy through phonon scattering. As the electric field in a particular zone increases, carriers eventually reach enough energy to impact ionize. The threshold for such processes has been reported to be of the order of 1.8 eV for electrons and 2.4 eV for holes, respectively [28]. It can, therefore, be expected that the highest possible energy levels for the excited electrons and holes will follow a distribution function around these values. Subsequent intraband relaxation processes may occur, for example relaxation of energetic electrons to lower energy levels in the conduction band, e.g., transitions of Type A in Fig. 2(c); and relaxation of energetic holes to lower energy levels in the valence band ptransitions of Type B in Fig. 2(c)].

5) Energetic electrons may also recombine directly with hot holes inside as well as outside the excitation zone and cause direct interband transitions of Type C, of approximately 2.8 to 3.2 eV, as demonstrated in Fig. 2(c).
6) Low-energy holes that are injected into the avalanching junction at the top of the valance ban from a nearby junction [G in Fig. 2(c)] may interact with energetic (hot) electrons generated in the avalanching (excitation) region of the junction through phonon-assisted recombination processes [F in Fig. 2(c)], resulting in transitions of Type D as illustrated in Fig. 2(c). The energy of these transitions is calculated as approximately 2.8 eV.
7) If a large number of mid-bandgap defects states are present in the depletion region, phonon-assisted transitions of Type E may also be stimulated, resulting in transitions of respectively 2.3 and 0.5 eV. Slight variations of the above may occur, since the transitions are greatly dependent on the position of the defect energy states within the energy gap.

A further hypothesis is that the respective transition probabilities may be enhanced by means of engineering carrier densities to populate specific regions in the energy band diagram, e.g., stimulating high-energy populations of F and G in the energy band diagram depicted in Fig. 2(c); increasing the dynamic carrier densities through the junction; and by introducing midband gap defect state densities in the junction.

The respective optical emission rates can be related by the following quantitative relationships: For the relaxation of excited electrons in the conduction band (intraband transitions)

$$L_{\mathrm{p}} = \alpha \mathrm{n}' N_c \tag{1}$$

where L_{p} is the relaxation rate leading to photon emissions, n' is the density of excited electrons, N_c is the density of available states at lower energy levels, and α is a relaxation probability which is dependent on various secondary parameters. A similar process holds for excited holes in the valence band.

For direct interband transitions, the relationship may be defined as

$$R_{\mathrm{p}} = \beta \mathrm{n}' \mathrm{p}' \tag{2}$$

where R_{p} is the so-called photonic recombination rate, n' and p' is the densities of energetic electrons and holes and β is a recombination probability constant.

For injection of secondary holes into the main avalanching junction

$$R'_{\mathrm{p}} = \Gamma \mathrm{n}' \Delta \mathrm{p} \tag{3}$$

where $\Delta\mathrm{p}$ is the density of additionally injected holes from the second junction, and γ is a corresponding recombination probability constant. The recombination probability constant depends on various secondary parameters such as density of available states, phonon energies available, and defect energy states.

Equation (3) clearly shows that much higher photon emission rates consequently an increase of orders of magnitude in light emission from the device may potentially be achieved if the injected hole density, $\Delta\mathrm{p}$, could be increased several orders of magnitude. This will greatly enhance the recombination processes corresponding to transitions of Type C and D and E. Such conditions can potentially be attained by means of the two junction device design as illustrated in Fig. 2. In avalanching junctions the current density through the excitation zone can reach 10^4 A cm^{-2} at 1 mA, with corresponding average dynamic carrier density of 10^{18} cm^{-3} to 10^{19} cm^{-3} for electrons exiting the junction [21]. The availability of minority carrier holes on the electron-emitting side of an avalanching $\mathrm{p}^+\mathrm{n}$ junction for this scenario is normally very low and of the order of 10^1 to 10^3 cm^{-3}. It follows that if the dynamic cool hole concentration in the neutral regions of the depletion region, or in the regions adjacently to the depletion layer, could be raised by five to six orders of magnitude, the recombination rate leading to optical emissions may correspondingly be raised by about six to seven orders of magnitude.

III. Modeling of Interband Photonic Transitions by Means of Depletion Layer Profing and Defect Engineering

Further analysis of the design concepts presented in Fig. 2, leads to different possibilities with regard to the choice of the dimension of the excitation zone, depletion layer thickness and size of the drift zone. On the other hand, the high doping density associated with the $\mathrm{p}^+\mathrm{n}$ junction, both the excitation zone and hot electron mean free path length (approximately 0.1 μm) [29] are very narrow, and are not really variable.

Fig. 3 gives a few common scenarios each of which favor interband photonic transitions. Intraband transitions are assumed to be also present but are not shown.

In Configuration I, a long depletion layer (typically 2–3 μm) and subsequent low gradient profile of the E-field are chosen. Injected holes travel subsequently long distances and are heated to high energy levels as they traverse through the depletion layer. This results in both the holes and emitted electrons being high in energy when they interact near the excitation zone, with subsequent little chance of direct interband recombination.

In Configuration II, the depletion layer is designed much shorter, resulting in a much "higher" heating of injected holes, before interacting with the emitted energetic electrons. If the heating profile is roughly of the same dimension of the 0.15 μm free path length of exiting high-energy electrons, electrons, and

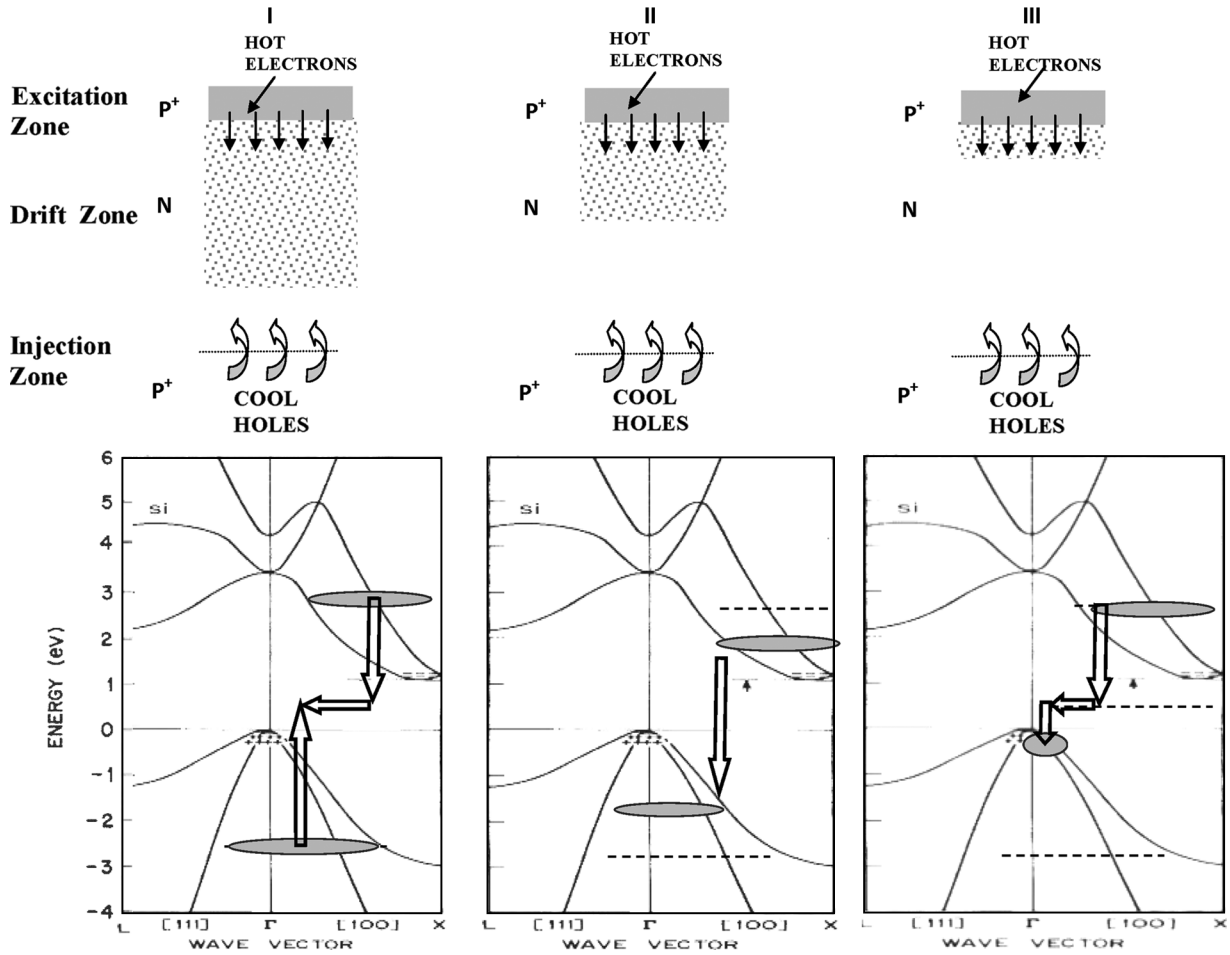

Fig. 3. Schematic presentation of projected dominant higher-than-bandgap photonic transitions in silicon band structure for different depletion layer profiling configurations in a p^+np^+ CMOS LED. (I) Long depletion layer design, (II) medium-range depletion layer design, and (III) very short depletion layer design.

holes can interact with each other over a much wider energy range.

Energetic (hot) electrons are losing their energy rapidly in the depletion layer, while the injected holes are gaining energy rapidly. It is therefore proposed that interband direct transitions may be the dominant transition processes if both the emitted carrier densities as well as the injected carrier densities are high.

The maximum transitions will occur at the minimum band-to-band edge of approximately 2.8 to 3.2 eV.

In Configuration III, Fig. 3, the depletion layer width is approximately of the same length as the mean free path of the emitted excited (hot) electrons of 0.1 μm, and the electric field profile is very steep. Injected holes will therefore still be in a very low-energy state when reaching the emitted hot carrier front. Both carrier densities may be high. Because of this specific energy distribution, inter band recombination may dominate, i.e., transitions from the maximum of the hot electron carriers (1.8 eV) to the minimum of hole energies ($\sim$0 eV), stimulating mainly defect-assisted interband transitions of approximately 2.8 eV [transitions of Type E in Fig. 2(c)].

Monte Carlo carrier transport simulations can provide information both on the carrier k-space and energy distribution as a function of the applied electric field strength in silicon. This information can be useful to better understand how the electric

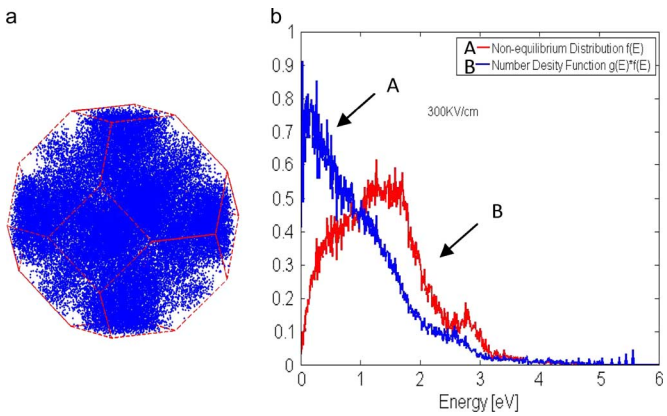

Fig. 4. Electron distribution in k-space and energy in silicon for an applied field of 300 kV cm^{-1} obtained from a Monte Carlo simulation. (a) K-space distribution in the first Brillouin Zone. (b) Energy distribution in the conduction band.

field changes the equilibrium distribution functions and as a possible way of confirming the above modeling. In Fig. 4(a), the electron distribution in k-space was evaluated in the presence of a high electric field of 300 kV cm^{-1}. The carrier distribution in the first Brillouin Zone (FBZ) clearly indicate that the carriers

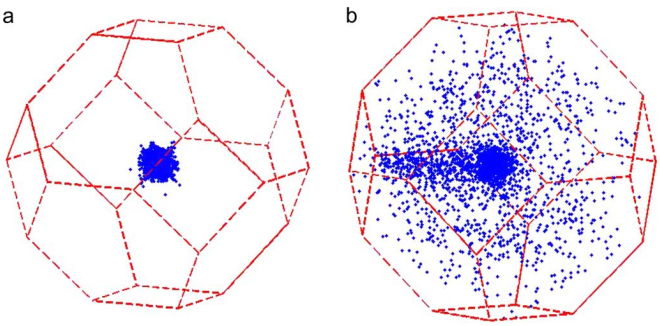

Fig. 5. Hole distributions in k-space in silicon for applied field strengths of (a) 10 kV cm^{-1} and (b) 300 kV cm^{-1}, obtained from a Monte Carlo simulation.

assume a wide variety of momentum states, quite evenly spread out over the whole FBZ.

Fig. 4(b) presents the calculated nonequilibrium probability distribution function (curve-A) and the nonequilibrium number density function (curve-B, defined as the product of the density of states and the nonequilibrium probability distribution function). As it can be clearly seen the number density function presents a broad maximum around a value of the carrier energy of 1.8 eV above the conduction band edge. Fig. 5 presents the calculated hole distribution in the FBZ for and applied electric field 10 kV cm^{-1} [Fig. 5(a)] and 300 kV cm^{-1} [Fig. 5(b)] applied along the (100) direction.

As it can be seen, at low electric field strength the majority of holes are located around the Γ point, near the top of the heavy and light hole valence bands. As the field strength is increased, holes tend to move away from the center of the FBZ toward higher energy states. predominantly in the heavy hole valence band.

This initial results seems to indicated that direct band-to-band transitions may indeed be possible under injection-avalanche conditions as explained above [transition Type C in Fig. 2(c)]. Furthermore, the considerable spread in momentum space, observed for both electrons and holes, may also be beneficial for the indirect transitions of Type E as in Fig. 2(c).

Fig. 6 attempts to couple some quantitative relationships to the above modeling. Fig. 6(a) gives the projected values for the respective carrier densities in the device under dynamic current carrying conditions as a function of distance in the device. The majority of electrons is generated in the excitation zone through multiplication processes. Since the ionization rate for electrons in the prevailing electric field at the n^+p interface during avalanche conditions is roughly twice that of holes [29], the excited electron density exiting the p^+n junction interface toward the n-side of the interface, is expected to be twice that of holes, resulting in mainly electrons being populated in the drift zone. If holes are injected into the drift zone from the forward-biased p^+n junction, it is expected that interaction between the respective carriers may occur through both energy relaxation and recombination processes in a so-called recombination zone as indicated, resulting in an eventual dynamic carrier density profile through the device as indicated. The estimated hot electron mean path length and profile are also indicated, which is of the order of 150 nm (0.15 μm) [29].

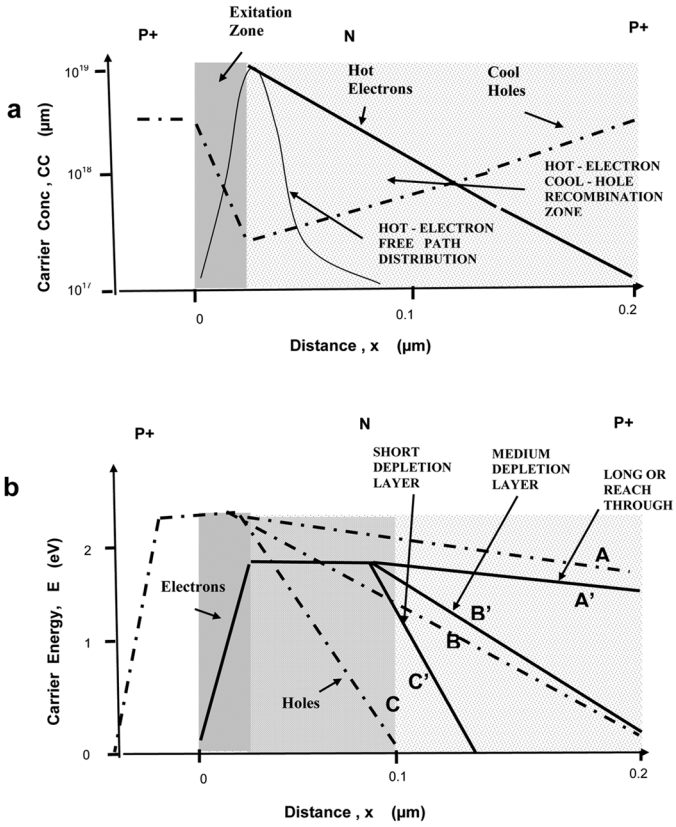

Fig. 6. Schematic presentation of the projected (a) carrier density versus distance in p^+np^+ injection-avalanche Si LED for a medium-range depletion layer and (b) the associated energy versus distance profiles for the carriers for short, medium, and long depletion layer designs, respectively.

Fig. 6(a) gives projected energy gain and energy loss profiles for the respective charge carriers as a function of distance in the device. Profiles for the energy of electrons (solid lines) and for the energy of holes (dotted lines) are indicated for the three different depletion layer scenarios

From this analysis, it can be concluded that a medium-sized depletion layer of approximately 0.4 μm (Configuration II in Fig. 4) with its associated projected energies of the carriers during diffusion is the most favorable device configuration for stimulating direct interband photonic transitions in the injection-avalanche device of Type C [Fig. 2(c)]. Both the energy values for the exited electrons and holes in the conduction and valance bands have moderate values of approximately 0.8 eV, respectively [Curves B and B′ in Fig. 6(b)], leading to possible direct interband transition of approximately 2.8–3.2 eV.

Secondly, it can be concluded from these profiles that a short depletion layer configuration will result in electron and hole energy profiles as indicated by Curves C and C′ respectively. This energy profile is the most favorable for stimulating transitions of Type D and E in Fig. 2(c), since it favors recombination of high densities of high-energy electrons with high densities of low-energy holes, as in Configuration III, Fig. 3. The optimum depletion layer thickness for this scenario is projected to be in the order of 0.3 μm. The current densities for both electrons and holes at this distance are also both high [see Fig. 6(a)], and therefore favors a very high recombination probability according to

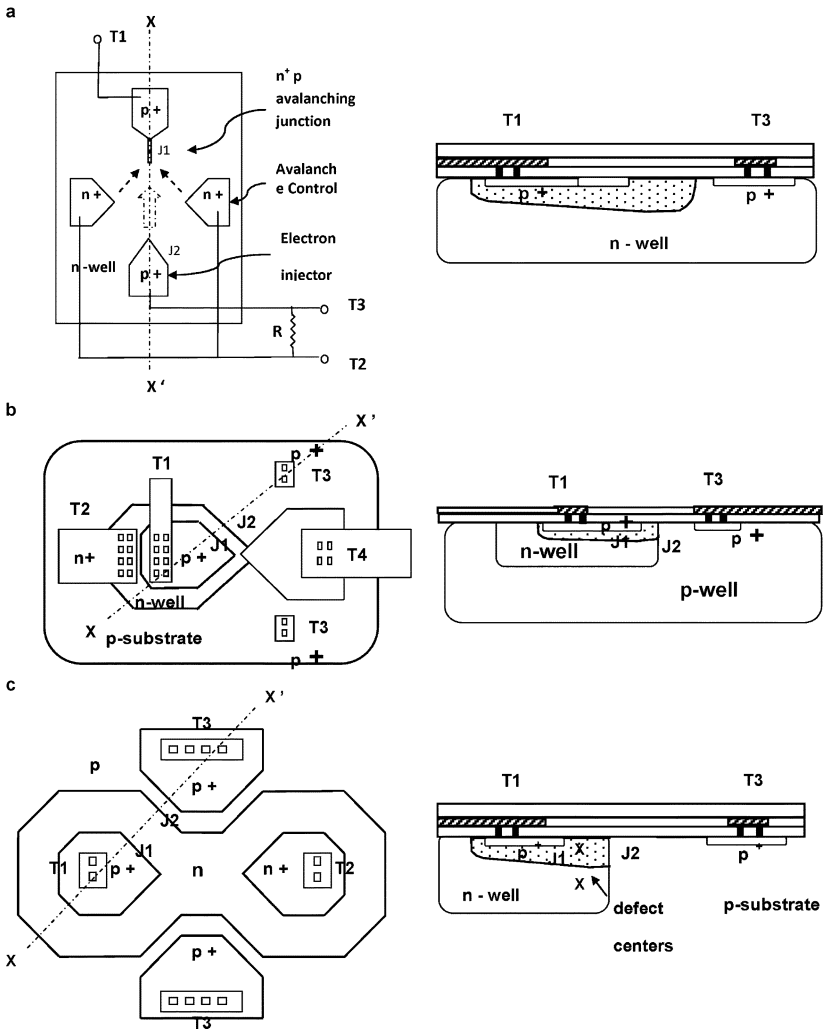

Fig. 7. Test structure designs for (a) p^+np^+ Injection-Avalanche Si LED with a long depletion layer design (TS1), (b) limited depletion layer design (TS2), and (c) medium depletion layer design plus defect engineering applied. The respective body and layer designations are applicable to 0.35 μm CMOS design and processing procedures.

(3). The E-field gradient for this configuration is calculated as 5×10^5 V cm$^{-1}\mu$m^{-1}.

The presence of midband defects states may enhance indirect recombination processes, [transitions of Type D in Fig. 2(c)] and in Configurations II and III, Fig. 3), since both the energy values and high densities of carriers present may favor these transitions according to (3). A variety of methods are currently available in order to introduce specific type of defects at specific locations and depths in silicon devices. These include: implantation of specific atom species followed by postannealing procedures in order achieve specific defect levels and active defect sate densities [30]–[32], direct wafer bonding in inert atmospheres [33], as well as current density stressing techniques [31], [34].

IV. Prototype Device Design

We have tested some of the above modeling by designing and realizing some prototype test structures.

Fig. 7(a) demonstrates a five bodied test structure (TS1), viz. a p^+ needle shaped body at terminal T1, facing a pentagon shaped p^+ body at terminal T3, and, diagonally opposite, two n^+ bodies, all embedded in a n-well substrate. If T2 is made the common (grounding) element and a negative bias voltage is applied to T1, a p^+n abrupt avalanching junction is formed at the needle-like tip with its depletion layer extending away toward the diagonal bodies at T2. If appropriate positive bias voltage is simultaneously placed on T3 relative to T1, the p^+n body at T3 (J2) is forward-biased and injects holes toward T1. The extend of the avalanche process in the main p^+n junction, as well as the extent of forward bias by T3, was controlled by means of an external bias resistor, R. Conditions were chosen such that for bias between T3 and T1, at low currents, the main current predominantly flowed between the diagonal n^+ (avalanche control) bodies, while at higher currents the main current flows between the injection body T3 and T1. The cross-section through the device along the dotted curve in Fig. 7(a) is shown adjacently. The distance from the injection point to the p^+n interface was 2.0 μm, therefore creating a medium heating profile for injected holes in a projected E-field gradient of 2×10^{-4} V cm$^{-1}\mu$m^{-1}.

Fig. 7(b) shows a test structure (TS2), comprising a small p^+ pointed body embedded in a n-well and again embedded in a larger p-well. The p^+n junction (J1) was reverse-biased by voltage biasing between T1 and T2.

By voltage biasing between T1 and diagonal terminals T3, the larger n-well p-well junction J2 was slightly forward-biased and hole carriers were injected into the depletion region at J1. By choosing the dimension and position of the n-well tub accurately, the extension of the depletion layer toward the T3 terminals was limited and a punch-through condition was reached. This created a medium-sized depletion layer of about 1 μm into which hole carriers were injected. Thus a device was created of which the depletion region width could be dimensioned to be in accordance with Configuration II or Configuration III in Fig. 3. A trapezium-shaped poly-Si layer and CMOS gate oxide layer was also placed on the structure (T4). This enabled a slight overlap of oxide over the reversed-biased junction J1 for specific investigation purposes, and allowing modification of the depletion region to only 0.5 μm, also corresponding to a punch-through condition and a heating profile of 5×10^5 V cm^{-1} μm^{-1}.

A further test structure, TS3, is demonstrated in Fig. 7(c). The p^+ body was again placed in a n-tub well. Biasing between T1 and T2 enables an elongation of the depletion layer toward T3. The width of the depletion region could again be varied in order to limit the depletion region width by choosing the dimensions and positioning of the larger n-well carefully. The main device current eventually flows predominantly between terminals T1 and T3, and creates a reverse-biased p^+n junction in series with a forward pn junction. The extent of the avalanche process at J1 was controlled by the voltage bias between T1 and T2. By stressing the junction at J2 beforehand according to a predetermined current density vs lattice stress calibration curve, some densities of defects could be introduced at the p^+n interface before operating the device. Hence the optical yield at J1 could be investigated when defect centers were present at J1.

All the above devices were realized using 0.35 μm state-of-the-art CMOS technology design and processing procedures [36].

V. Experimental Results and Discussions

Fig. 8 demonstrates some of the most important results observed. Fig. 8(a)–(c) shows bright field optical micrographs of the test structures TS1 to TS3 as seen through an optical microscope with visible light and at very high magnification. Adjacently, in Fig. 8(d)–(h), corresponding optical emission performances are shown as taken under dark field conditions with a CoolPix Model 4500 Nikon charge-coupled device (CCD) digital camera with recording facilities.

Fig. 8(d) shows the TS1 version of the device under operation for pure avalanching conditions at J1 with no current injected into the junction J1. The extent of avalanching and light emission around the peripheries of the p^+n junction are clearly observed. At the tip of the body a much brighter zone can clearly be identified. This phenomenon is attributed to higher optical emission intensity as a result of current density confinement according to previous interpretations [21].

Quantitative analyses of the optical emission versus electrical power input to the device as in Fig. 8(a) reveal an interesting two sloped curve which clearly indicate that a mechanism change occurred for the device at about 10 mW. This mechanism is attributed to a partial collapse of the depletion layer as it occurred

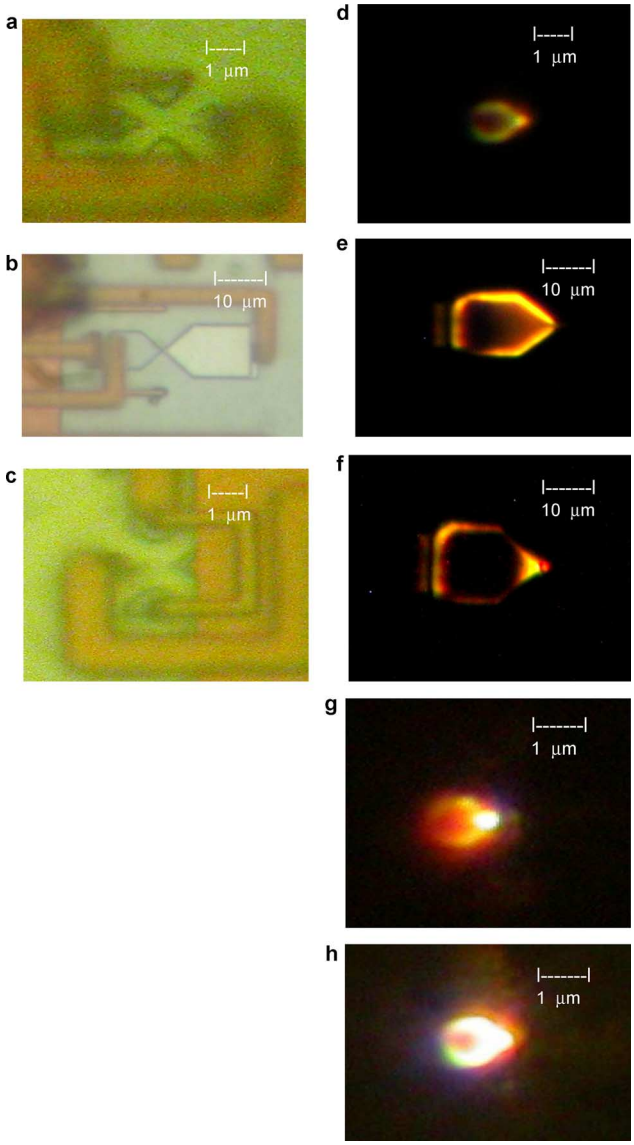

Fig. 8. Bright field and dark field photomicrographs for Si injection-avalanche CMOS Si LEDs. (a) Test Structure 1 (TS1) (b) TS2 with poly-Si layer added. (c) TS3 structure (d) TS1 for pure avalanche operating conditions for 15 V and 1 mA. (d) TS2 for 8 V and 2 mA operation. (f) TS2 plus poly-Si test structure at 15 V and 1 mA operation. (g) TS3 for 8 V and 1 mA operation under mixed avalanche-injection operation (80–20%). (h) TS3 for 8 V and 3 mA operation under full injection conditions.

in three-terminal transistor devices for injection conditions in traditional emitter to base configurations [37]. The optical yield for only avalanche operation at low current levels is about two photomultiplier units (PMUs) per milliwatt of electrical input power, while at higher current levels (injection conditions), the slope is higher and is of the order of about 4 PMUs per milliwatt.

Fig. 8(e) shows the characteristics for the TS2 version device for roughly similar operating conditions as in TS1. In this case the total p^+n junction length and pn^+ junction area were much larger [see dimensions in Fig. 8(b)]. Particularly noticeable, is the much higher brightness along the right-hand side periphery of the device, where, according to our analyses, much higher injection current of holes occurred into the junction, as compared to peripheries on the left-hand side which is closer to the

avalanche control terminal T2 and which represents light emission corresponding to pure avalanching conditions.

Quantitative analyses as in Fig. 9(b) show a clear changeover in mechanism with a generated higher optical yield of approximately 20 PMUs per milliwatt of input electrical power for this device at an estimated 50% hole injection conditions. It is important to note that because of the larger dimension of the p^+ layer in this device, a large injection current component was injected toward the bottom part of the p^+ layer embedded in the n-well cross-section layout [Fig. 7(b)] and did not contribute toward light emission at the p^+n peripheries. Considering these conditions, as well as the fact that the current density at the p^+n peripheries was much lower during injection conditions than during pure avalanche, the inherent optical yield during injection-avalanche for smaller depletion layer configuration is derived to be much higher. From the data curves as derived in Fig. 9(b), the projected internal optical yield for the 1-μm limited depletion layer conditions as in TS2, Fig. 8(b), is anticipated to be of the order of 400 PMUs per milliwatt of input electrical power (dotted curve C, higher end). This curve was derived by means of the following approximated expression:

$$\mathrm{N_{pp}} = \frac{\Delta PMU(O)}{Vd\Delta Id} \times \frac{A_t}{A_c} \tag{4}$$

where $\mathrm{N_{pp}}$ is the projected internal power conversion efficiency; $\Delta PMU(O)$ is the incremental optical power output in PMU units; V_d is the bias voltage for the device at the change in slope; ΔI_d is the incremental current change at change in slope; A_t is the total depletion layer cross-section area that absorbs injected current; and A_c is the depletion layer area that contributes toward light emission.

Furthermore, experiments were conducted with the same device structure but with a poly-Si gate overlapping the n-well as in Fig. 8(b). When a leakage path was set up through the oxide layer, current could be injected into the depletion layer only 0.5 μm from the p^+n junction interface. Particularly noticeable was a very bright (whitish in color) but very small spot [Fig. 8(f)]. Also noticeable is a fainter (more reddish in color) second spot at the right-hand edge, a very short distance away. The magnitude of brightness of the first spot is at least one order of magnitude higher than the periphery emissions when the intensity profiles are considered. It is our opinion that the spot emission originates from the interaction of exciting high-energy electrons at the p^+n interface with injected holes into the depletion region only 0.5 μm away from a large sea of electrons as generated by the avalanching junction at the p^+n interface. The curves in Fig. 10(a) as well as the observation of the formation of secondary light spots with increase in bias voltage, indicate that some of the light emission processes in this device was much more efficient than in previous devices. The projected contribution of the brightest spot to the total emitted power is indicated by the dotted curve. Investigation of the total emitted intensities versus area revealed that there was a high leakage current present in the device due to avalanche conditions in the rest of the p^+n periphery.

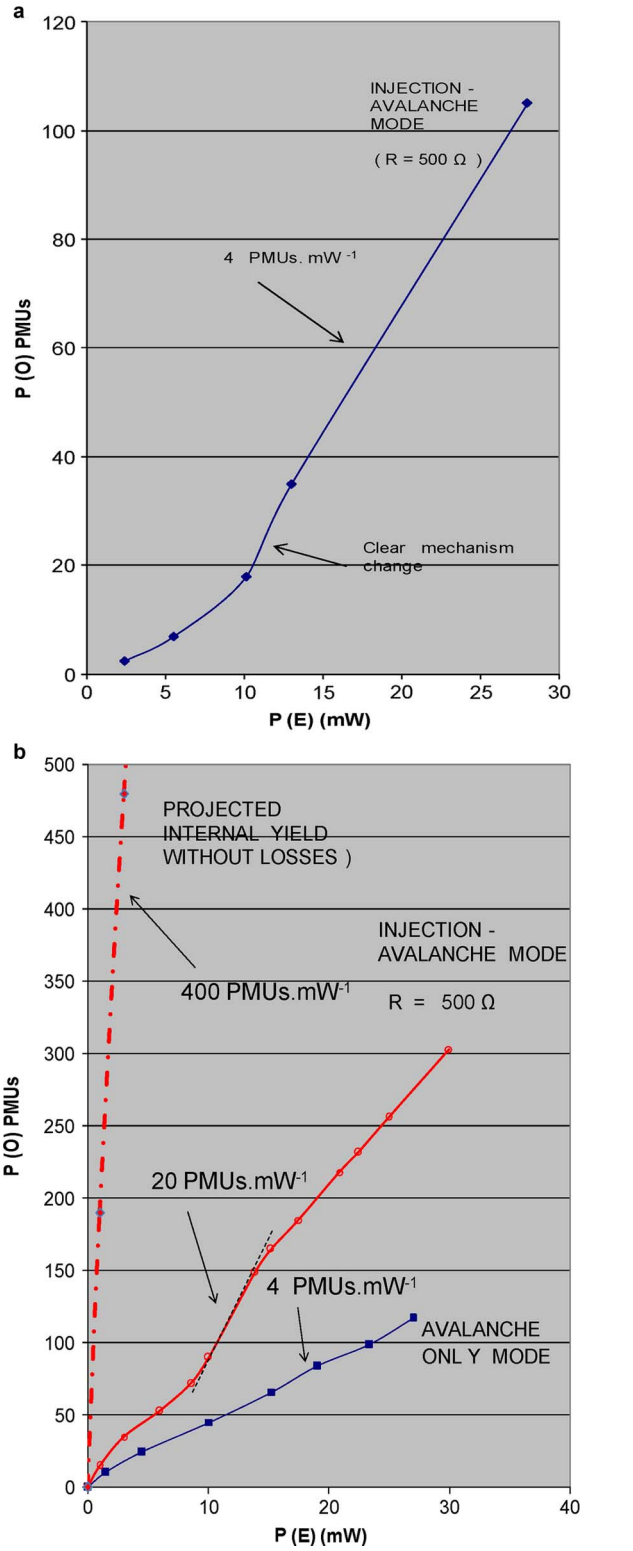

Fig. 9. (a) Optical power versus electrical input power performance for TS1 in injection avalanche mode of operation and depletion layer width 2 μm. (b) Optical power versus electrical input power performance for TS2 with depletion layer width, 1 μm. The projected internal optical yield without losses due to electron-hole interaction in the device is indicated by means of the dotted curve.

After calculations, the inherent optical yield for the bright spot was projected to be of the order of 1000 PMUs per milli-

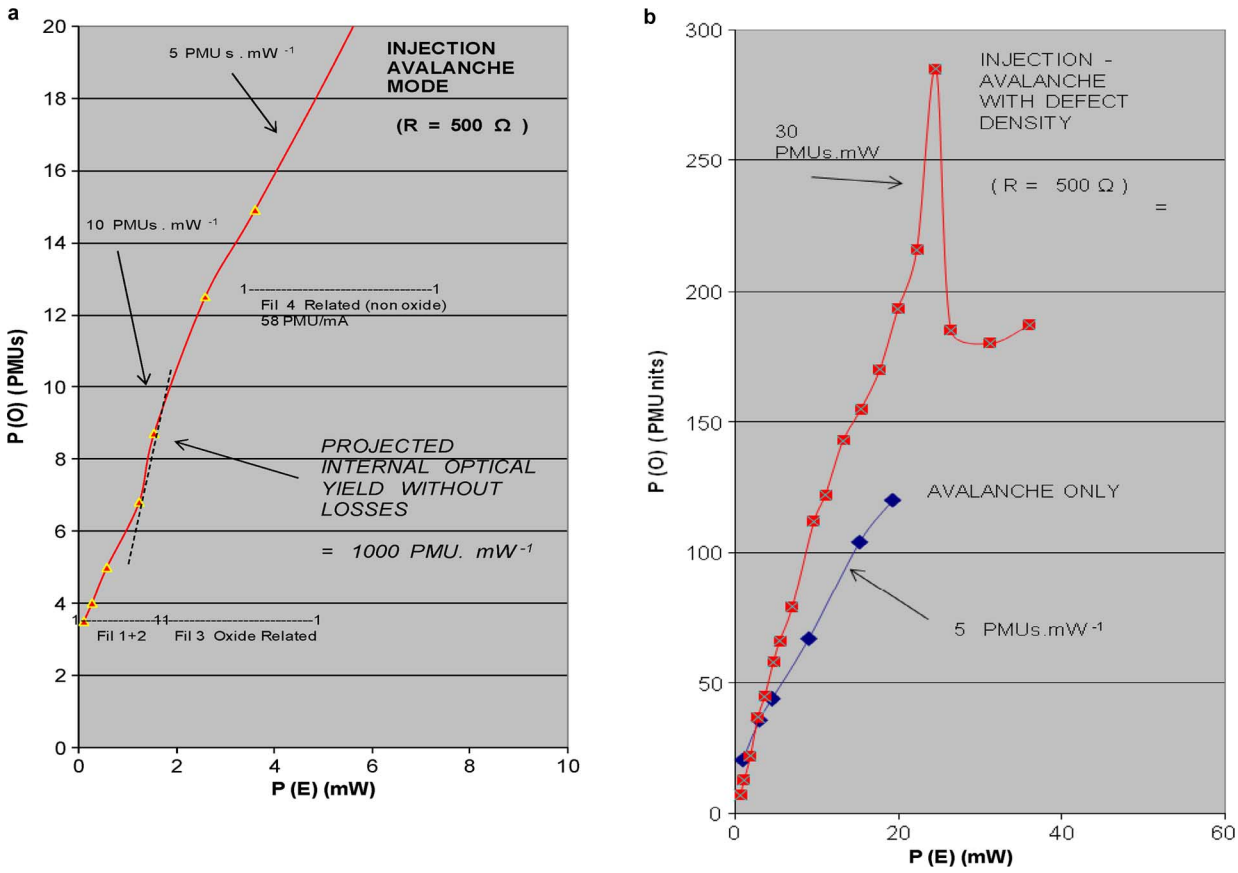

Fig. 10. (a) Optical power versus electrical input power performance for TS2-Poly Si Injection Test Structure with depletion layer width of 0.5 μm. (b) Optical power versus electrical input power performance for TS3 for injection-avalanche mode of operation and with defect densities introduced into the depletion layer. The localized optical yield as emitted due to electron-hole interaction and defect interaction is indicated.

watt of input electrical power, if it is assumed that only about 50 μA contributed to the spot emission. The following approximated expression was used in this calculation:

$$\mathrm{N_p(Local)} = \frac{\Delta PMU(O)}{V_d \Delta I_d} \times \frac{A_t}{A(Spot)} \tag{5}$$

where $\mathrm{N_p(Local)}$ is the local power conversion efficiency; $\Delta PMU(O)$ is the incremental optical power output in PMU units; V_d is the bias voltage for the device at the change in slope; ΔI_d is the incremental current at change in slope; A_t is the total area that contributes to light emission; and $A(Spot)$ is the light-emitting area for the spot causing the change in light emission.

Fig. 8(g) and Fig. 10(b) show emission phenomena that was observed for Test Structure 3, Fig. 7(c), into which defect densities have been introduced near the p^+n interface. Again the presence of a bright spot is observed which is much brighter than the areas which are in pure avalanche light emission mode of operation (seen toward the left and right along the p^+n periphery). Particularly noticeable was the growth of the spot intensity (almost as a flare explosion) as current was increased. This again indicated a further change of light producing mechanism as the net increase in detected optical power now comes from only a very small area in the device of approximately $0.1\ \mu\mathrm{m} \times 0.1\ \mu\mathrm{m}$. Quantitative investigations of optical yield as a function of incremental electrical power increase and as a function of contributing area to total light-emitting area yields an optical yield of approximately 50 PMUs per milliwatt external and a projected 1000–2000 PMUs per milliwatt of electrical input power inherently per defect generating area if losses are ignored (several cases were investigated). In this particular case the particular injection conditions into the depletion layer has not been optimized which implies that the eventual emission could still be much improved if the device is further optimized.

An interesting observation is the decrease in emission in the curve in Fig. 10(b) as the current is increased further. This is currently attributed to energy differences in the injected carriers that occur at higher injection current conditions that lead to nonoptimized recombination effects for transitions of Type D in Fig. 2(c). The effect is currently further researched.

Fig. 8(h) shows an optimized version of the operation of the TS3 device with the p^+n junction, needle tip device in strong avalanche and with very high hole current injected (approximately 2 mA) into the avalanching junction, which we attribute to a culmination and a combination of all the effects that contribute toward higher optical emission in the injection-avalanche structures as observed so far, i.e., optimum depletion profile, carrier density balance and defect densities introduced. The clear higher intensity at the needle tip region is apparent, as well as the definitely much more blue-whitish color of emission as compared with pure avalanching light-emitting

junctions. The particular operating conditions is 8 V, 2 mA, and with approximately 1.6 mA of the current measured as injected current through the injector contact, T3, as in Fig. 7(a). The depletion layer thickness (injection distance) in this device was of the order of 1 μm and this parameter can hence be further optimized.

The optical emission per area (intensity) of the light emission as emitted is very promising, and is of approximately 10 nW μm^{-2}.

A progressive increase in total optical emission as well as in localized intensities are demonstrated in Fig. 8(d)–(h) at roughly similar operating voltages and currents.

VI. Some Spectrographic Observations

Fig. 11 shows typical spectrographic information as measured for our injection-avalanche devices. Fig. 11(a) shows the wavelength spectrum of the emitted light as observed for a pure avalanching junction of type TS1, while Fig. 11(b) shows the change observed in the spectra as a function of increase in injection current for structures of type TS2. The spectra has been corrected for absorption effects as they occur in the silicon subsurface as a function of wavelength. The scales are representative of the relative intensities as observed.

Spectroscopic measurements of the emitted light reveals clear emission peaks at 1.8, 2.2, 2.4, and 2.8 eV in the 450–885 nm wavelength region. A similarity of the avalanche-based curves is observed (1-mA curve in (a) and 0.07 mA in (b) while very prominent changes are observed for the higher current curves [3 and 10 mA in Fig. 11(b)] when the injection current component was present. Very significant, is the growth of the 2.3 and 2.8 eV peaks. High injection current losses to nonavalanching areas (as outlined earlier) should however be appreciated.

In overall, the following conclusions were derived from spectroscopic information.

1) The observed 1.8 eV photonic emissions as observed in the spectra may correspond with intraband relaxation mechanisms within the conduction band [Transition Type A, Fig. 2(c)] as a result with interaction of host Si atoms. The value of 1.8 eV corresponds with energy required for ionization of host silicon atoms by electrons [28].
2) The observed 2.4–2.5 eV photonic emissions as observed in the spectra may correspond with intraband relaxation mechanisms [Transition Type B, Fig. 2(c)] within the conduction band as a result of interaction with host Si atoms.
3) The observed increase in the 2.8 eV energy peak in Fig. 11(b) as a function of injection current may indicate that band-to-band transitions of Type C and Type D s described in Fig. 2(c) and Fig. 3 Configuration III may indeed be present. Since the interband transition probability is proportional to the both the carrier densities n' and Δp, as predicted by (3), the 2.8 eV peak should definitely grow with increase in hole injection current. This is indeed observed.
4) The presence of a clear emission peak at 2.2 eV indicate that the phonon-assisted transitions from the 1.8 eV energetic position for electrons, to defect states in the middle of the band gap are highly feasible and it may indeed be stimulated by interband acoustical phonon-assisted transitions of Type E, as in Fig. 2(c). According to (3), these transitions will also be dependent on the product of the densities of the excited electrons as well the density of injected low-energy holes. A nonlinear growth of this peak is therefore expected. From the results shown in Fig. 11(b), this seems to be observed, considering the growth of the 2.2 and 2.8 eV peak as a function of current. This observation also correlates with the nonlinear increase in the optically emitted power as function of current at the higher current levels when predominantly injection current as observed in both Fig. 9(a) and Fig. 10 further confirms this phenomenon. Both the latter two physical trends thus support the 2.2 eV defect- and phonon-dependent optical emissions.

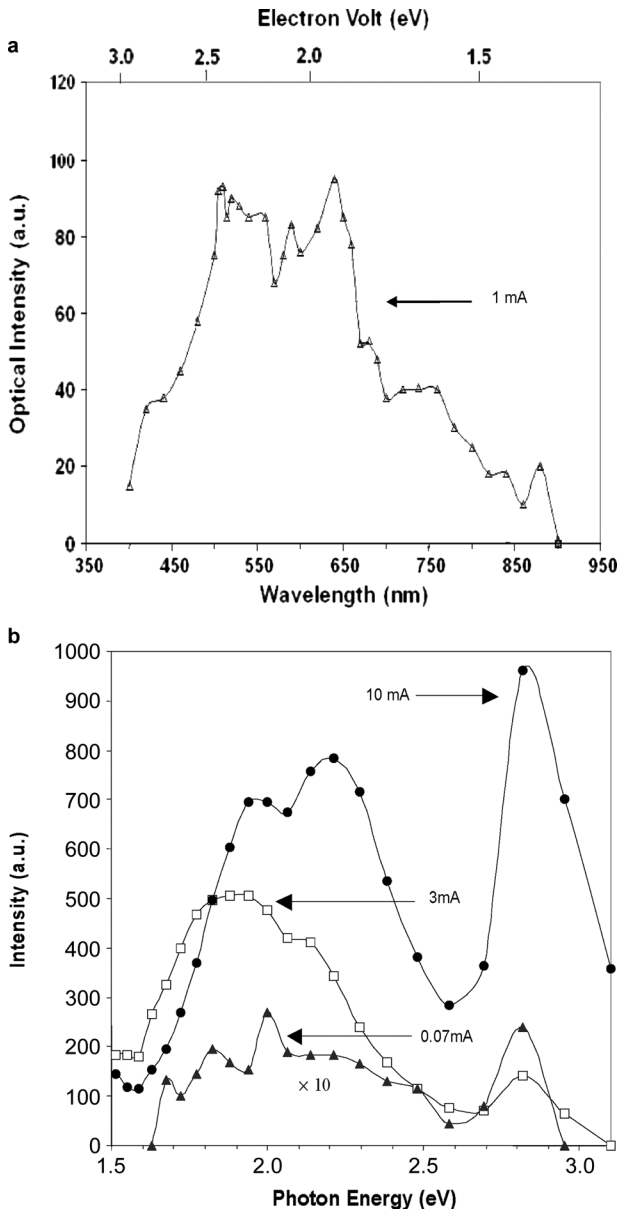

Fig. 11. Intensity spectra for optical emissions for (a) CMOS LED for pure avalanche mode of operation. (b) Intensity versus photon energy for operation for a CMOS LED in the injection-avalanche mode of operation for various injection current levels. The wavelength emissions have been corrected to present optical yields at the generation sites.

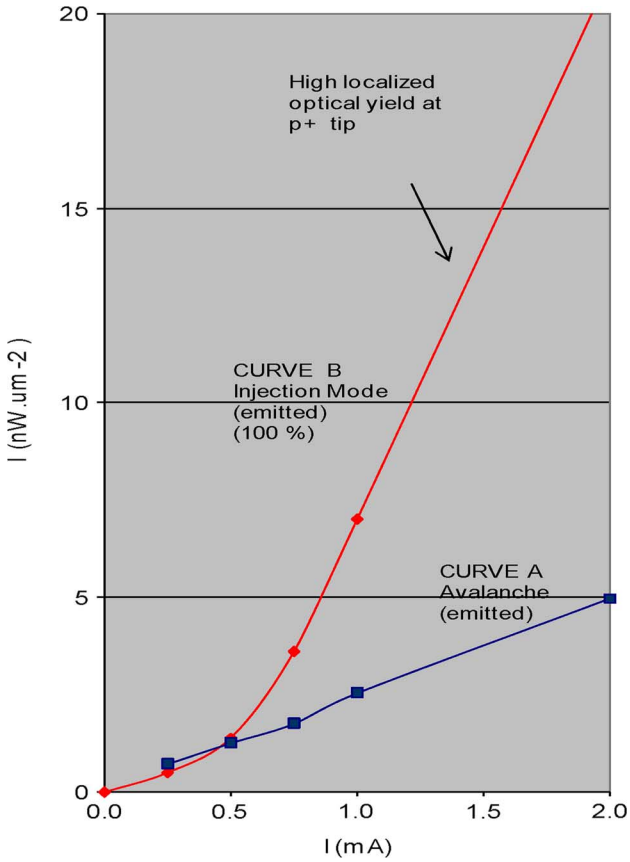

Fig. 12. Optical intensity versus electrical current performance for TS3 for 20% avalanche current and 80% injection current.

5) Since the detector had quite a broad and even detectivity in the range 450–850 nm, the increase in the 2.3 and 2.8 eV peaks were mainly responsible for the changes in total emission intensity as observed in Fig. 9 and Fig. 10, and the curves are therefore, reasonably representative of the injection effects.

VII. Some Quantitative Derivations

Using calibrated external illumination sources, both the CCD camera as well as the photomultiplier could eventually be calibrated. This enabled conversion of the PMU photonic yields units into more quantitative values. The photomultiplier tube was calibrated as approximately 10 nW per 100 PMUs for the particular measuring conditions used. Using photographic white levels and objective acceptance angles as a measure, the optically emitted power per unit area on the devices (i.e., intensity) could also be derived from the CCD camera photomicrographs. Fig. 12 gives typical characteristics as derived. For example, an intensity value of up to 100 nW μm^{-2} could be derived at 8 V and 1 mA operation for a 0.1 μm^{-2} emitting area for the TS2 polysilicon device.

Considering the optical power outputs per unit area as in Section III with respect to current and voltage bias conditions (1 nWμm^{-2} at 1 mW for single junction mode of operation and 10 nWμm^{-2} at 1 mW for injection mode of operation), estimations of the respective external and internal power conversion efficiencies could be made. This was achieved by taking the 2.2 eV (650 nm) peak as main reference peak. Calculations using the refractive indices of n = 3.48 for Si, an absorption factor for Si of 0.59 at 650 nm, and internal reflection considerations as the light moves from higher refractive indices to lower refractive indices surface layers, reveals an emission factor of 0.21 for emission from Si to SiO_2. Calculations using the refractive indices of n = 1.4 for SiO_2, 2.5 for Si_3N_4 an absorption factor of 0.3 for Si_3N_4 layer, and considering 1-μm thickness layers, yield an emission factor of 0.25 for transmission through the SiO_2 and Si_3N_4 surface layer to ambient air. The Si_3N_4 layer contributes to an absorption loss of about 0.3. The total emission factor from the subsurface n^+p-avalanching junction to air is therefore 1.5×10^{-2}.

This implies that the internal power conversion efficiency is of the order of 10^{-6} for a single avalanching junction; and of the order 10^{-5} to 10^{-4} for two junction injection mode of operation. However, the injection mode of operation suffers from current contribution as well as current density reduction loss through the active avalanche-injection light regions of part of the device of the order of 10^{-2}. The injection current does not conduct only through the needle tip at J1 but through the whole n^+p reverse bias junction including the bottom surface area of the n^+p embedded region as well, Fig. 7(a). This implies that the maximum achievable power conversion efficiency for injection mode of operation alone may be as high as 10^{-3} to 10^{-2}. This is much higher than the previous determined values of approximately 10^{-6} for single junction avalanche only devices [18], [19]. The authors are currently pursuing with realizations of these devices on Silicon on Insulator (SOI) structures in order to minimize the substrate-related injection losses.

In summary, the experimentally realized as well as the projected optical yield as a results of injection-avalanche mechanisms are presented in Table I. Particularly promising is the optical yield that can be realized with a combination of depletion layer and defect engineering with TS3 if the device designs.

VIII. Comments on Speed of Silicon CMOS Avalanche LEDs and for Injection-Avalanche CMOS LEDs

The avalanche impact ionization process in semiconductors is generally considered to be inherently a very fast process. The speed of operation of avalanche breakdown mode is determined by the RC time constant of the device, as well as the carrier transit time through the depletion region. With the dynamic on-resistance of the pn junction in avalanche in the tens of kilo-ohms range and the reverse-biased junction capacitance in the range of femto farads, the RC time constant will be in the range of tens of psec. This will be sufficient to produce modulation in excess of 10 GHz. Similarly, the transit time of excited carriers drifting at approximately the carrier saturation velocity of 10^7 cm/s through the length of the depletion region (0.4 μm in our case) will also be in the range of 10 psec. Switching speeds faster than 10 GHz have already been experimentally demonstrated for silicon avalanche electroluminescence devices [8], [35].

Our two junction injection devices will exhibit the same switching speed in the avalanching junction, but the forward-biased junction injecting carriers toward the avalanching junction will add an additional time delay to the speed response. This is due to the relatively slow diffusion of the injected carriers toward the avalanching junction in the charge neutral

TABLE I
OPTICAL YIELDS REALIZED, OPTICAL INTENSITIES REALIZED, AND INTERNALLY PROJECTED OPTICAL YIELDS FOR THE VARIOUS Si CMOS LED TEST STRUCTURE DESIGNS UNDER SPECIFIC OPERATING CONDITIONS

DESIGN	TOTAL EXTERNAL OPTICAL YIELD (nW mW $^{-1}$)	PROJECTED LOCAL INTERNAL OPTICAL YIELD (INJECTION RELATED) (nW mW $^{-1}$)	EMITTED OPTICAL INTENSITY (Maximum as in 0.1 μm^2 areas) (nW μm^{-2})
TS1 p^+np^+ injection-avalanche Only avalanche mode of operation	0.2		1
TS1 p^+np^+ injection-avalanche mode (100 % injection current)	0.4	10	10
TS2 p^+np^+ injection-avalanche mode (100% injection current) (depletion layer limitation = 1 μm)	1	40	15
TS2 p^+np^+ injection-avalanche (PolySi avalanche control) (80% injection current) (depletion layer limitation = 0.5 μm)	0.4	100	100
TS3 p^+np^+ injection-avalanche (100% injection current) (depletion layer limitation = 2 μm) (defect engineering introduced by means of current stressing beforehand , 10^5 A . cm^{-2}, 1 minute)	2	200	100

region. If the distance between the forward-biased injection junction and the reverse-biased avalanching junction depletion region can be made short, this diffusion time can be minimized. The transit time of diffusing carriers through a region of length W is given by

$$\tau = \frac{W^2}{2\mu\frac{kT}{q}} \tag{6}$$

under low injection level conditions, with μ the mobility of the injected carriers.

In the case of electrons being injected, and a typical spacing of W $= 0.5$ μm, the transit time for the diffusing carriers is in the order of 50 psec. Adding this to the 20 psec time constant of the avalanching junction, a combined switching speed in the range of 10 GHz may still attainable for the two junction carrier injection light-emitting device.

IX. CONCLUSIONS

This paper has shown that the optical emissions for two junction injection-avalanche-based silicon light-emitting devices are dependent on depletion layer profiling as well as on the introduction of defect centers in the depletion layer.

In our opinion a much better understanding of the basic mechanisms that is responsible for higher than bandgap light emission mechanisms in silicon has been achieved.

The obtained experimental observations sufficiently supports enhanced inter band photonic transitions according to the hypotheses that injected low-energy holes can interact with higher energy electrons and stimulate enhanced optical emission transitions of mainly 2.2 and 2.8 eV. Modeling proposed that an electric field gradient of approximately 4×10^5 V cm^{-1}, as well as preferred injection distance of low-energy holes directly into the depletion region of 0.4 μm will optimize such transitions.

Furthermore, evidence had been obtained that defect centers introduced by current stressing can significantly enhance the optical emission transitions. Our current device design and understanding of the physical mechanisms involved also offers tweaking of the emitted radiation to the 700–800 nm and even to the infrared regime.

Indications have been obtained that the inherent and internal yield of up to 100 nWμm^{-2} were derived for the injection-avalanche mode of operation. Therefore the future external op-

tical power yield as associated with these devices could be much higher if further optimization is implemented with regard to device design. The absorption and emission losses from the surface layers in the current structure still offer major challenges.

Particularly promising is the optoelectronic application feasibilities, especially in CMOS integrated circuitry, as have emanated from this work. The results presented in this paper reports extraction of optical intensities to 1–10 nW μm^{-2}, while internal effeciencies of up to 100 nWμm^{-2} can be derived with our injection-avalanche technology. Previous results using single junction devices operating in the avalanche light-emitting mode typically yielded externally detected intensities of only 0.1–1 nW μm^{-2} [22] This implies that these optical powers may be transferred to adjacent structures in CMOS integrated circuitry for diverse on-chip signal processing and for example wave guiding or electro-coupling applications. Previous analyses showed that, although the threshold of small dimension pn detectors in CMOS structures are of the order of pico-Watts, a few nano-watt of transferred optical power, either internally or to the external environment, is sufficient to extract clean signals in the low-frequency regime [39], [40]. Further analyses show that progressive higher levels of incident power are needed at higher in order to compensate for losses which occur with transimpedance type amplifier for frequencies ranging into the higher frequency regimes. Recent analyses has shown that amplification of optically detected signals of 10–100 nW incident on 10×10 μm CMOS detector and transimpedance amplifier configurations of up to 1 GHz [40].

It seems, therefore, that about 1 nW of optical intensities per μm^{-2} are internally needed in order to make diverse electro-optical applications possible in CMOS integrated circuitry. Our demonstrated localized optical yields of 100 nW μm^{-2} and realized external emitted intensities of 1–10 nWμm^{-2}, for normal CMOS device operating conditions of a few volts and about one mA, therefore, makes diverse electro-optical applications already feasible. The current emission levels of our CMOS Si injection-avalanche LEDs of 10–100 nW μm^{-2}. is therefore about three to four orders of magnitude higher than the minimum low-frequency detectivity of standard CMOS detectors of comparable dimension as outlined above.

This implies that diverse electro-optical applications using this technology, as outlined above, are indeed possible. Some of the first novel applications of the technology may be in Micro Optical Electromechanical Sensor (MOEMS) devices, which will offer the realization of diverse sensor devices, from physical parameter sensing such as temperature, vibration, acceleration, rotation, to more advance applications such as absorption, reflection, spectrometric analysis of gases and fluids. This will add considerable functionality to existing CMOS chip packages which is a general trend in the current IC technology after the limitations due to scaling have been reached.

ACKNOWLEDGMENT

The financial support of the National Research Foundation in South Africa, as well as the utilization of laboratory facilities at the Carl and Emily Fuchs Institute for Microelectronics (CEFIM) at the University of Pretoria is gratefully acknowledged.

REFERENCES

[1] E. A. Fitzgerald and L. C. Kimerling, "Silicon-based technology for integrated opto-electronics," *MRS Bull.*, pp. 39–47, 1998.
[2] R. Soref, "Applications of silicon-based optoelectronics," *MRS Bull.*, pp. 20–47, 1998.
[3] D. J. Robbins, "Editorial comments on volume "silicon opto-electronics" at Photonic West Annual Conference at San Jose, California, U.S.A.," in *Proc. SPIE*, 2000, vol. 3953.
[4] P. M. Fauchet, "Progress toward nanoscale silicon light emitters," *IEEE J. Sel. Topics Quantum Electron.*, vol. 4, no. 6, pp. 1020–1028, Nov./Dec. 1998.
[5] N. Savage, "Linking with light," *IEEE Spectrum*, vol. 39, no. 1, pp. 32–36, Jan. 2002.
[6] L. W. Snyman, K. A. Ogudo, M. du Plessis, and G. Udahemuka, "Application of Si LED's (450 nm–750 nm) in CMOS integrated circuitry based MOEMS—Simulation and analyses," in *Proc. SPIE*, Feb. 2009, vol. 7208, p. 72080C.
[7] K. Wada, "Electronics and photonics convergence on silicon CMOS platforms," in *Proc. SPIE*, 2004, vol. 5357, p. 16.
[8] A. Chatterjee, B. Bhuva, and R. Schrimpf, "High-speed light modulation in avalanche breakdown mode for Si diodes," *IEEE Electron Device Lett.*, vol. 25, no. 9, pp. 628–630, Sep. 2004.
[9] W. G. Ghynoweth and K. G. McKay, *Phys. Rev.*, vol. 102, pp. 369–376, 1956.
[10] R. Newman, "Visible light emission from a silicon p-n junction," *Phys. Rev.*, vol. 100, pp. 700–703, 1955.
[11] J. Bude, N. Sano, and A. Yoshii, "Hot carrier luminescence in silicon," *Phys. Rev. B*, vol. 45, no. 11, pp. 5848–5856, 1992.
[12] J. Kramer, P. Seitz, E. F. Steigmeier, H. Auderset, and B. Delley, *Sens. Actuators*, vol. A37–38, pp. 527–533, 1993.
[13] L. Carbone, R. Brunetti, C. Jacoboni, A. Lacaita, and M. Fischetti, "Polarization analysis of hot-carrier emission in silicon," *Semicond. Sci. Technol.*, vol. 9, pp. 647–676, 1994.
[14] Lacaita, F. Zappa, S. Bigliasrdi, and M. Manfredi, "On the Brehmstrahlung origin of hot-carrier-induced photons in silicon devices," *IEEE Trans. Electron Devices*, vol. 40, no. 2, pp. 577–582, Feb. 1993.
[15] N. Akil, S. E. Kerns, D. V. Kerns, Jr., A. Hoffmann, and J.-P. Charles, "A multi-dimensional model for photon generation in silicon junctions in avalanche breakdown," *IEEE Trans. Electron Devices*, vol. 46, no. 5, pp. 1022–1027, May 1999.
[16] L. W. Snyman, M. du Plessis, E. Seevinck, and H. Aharoni, "An efficient, low voltage, high frequency silicon CMOS light emitting device and electro-optical interface," *IEEE Electron Device Lett.*, vol. 20, no. 12, pp. 614–617, Dec. 1999.
[17] M. du Plessis, H. Aharoni, and L. W. Snyman, "Silicon light emitting devices in standard CMOS technology," in *Proc. IEEE Conf. Anuala de Semiconductoare (CAS)*, 2001, pp. 231–238.
[18] L. W. Snyman, H. Aharoni, M. du Plessis, and R. B. J. Gouws, "Increased efficiency of silicon light emitting diodes in a standard 1.2 micron complementary metal oxide semiconductor technology," *Opt. Eng.*, vol. 37, pp. 2133–2141, 1998.
[19] L. W. Snyman, H. Aharoni, M. du Plessis, J. F. K. Marais, D. van Niekerk, and A. Biber, "Planar light emitting electro-optical interfaces in standard silicon complementary metal oxide semiconductor integrated circuitry," *Opt. Eng.*, vol. 41, pp. 3230–3240, 2002.
[20] M. du Plessis, H. Aharoni, and L. W. Snyman, "Two- and multi-terminal CMOS/BiCMOS Si LED's," *Opt. Mater.*, vol. 27, pp. 1059–1063, 2005.
[21] L. W. Snyman, H. Aharoni, and M. du Plessis, "Two order increase in the quantum efficiency of silicon CMOS n+pn avalanche-based light emitting devices as a function of current density," *IEEE Photon. Technol. Lett.*, vol. 17, no. 10, pp. 2041–2043, Oct. 2005.
[22] M. du Plessis, H. Aharoni, and L. W. Snyman, "Spatial and intensity modulation of light emission from a silicon LED matrix," *IEEE Photon. Technol. Lett.*, vol. 14, no. 6, pp. 768–770, Jun. 2002.
[23] L. W. Snyman, M. du Plessis, and H. Aharoni, in *Proc. IEEE Int. Symp. Industrial Electronics (ISIE 2005)*, 2005, vol. 3, pp. 1159–1169.
[24] L. W. Snyman, M. du Plessis, and H. Aharoni, "Three terminal optical sources (450 nm–750 nm) for next-generation silicon CMOS OEIC's," in *Proc. 12th Int. Conf., Mixed Design of Integrated Circuits and Systems (MIXDES'2005)*, Krakov, Poland, 2005, pp. 737–747.
[25] L. W. Snyman, M. du Plessis, and H. Aharoni, "Two order increase in the optical emission intensity of CMOS integrated circuit LED's (450–750 nm) comparison of n^+pn and p^+np designs," in *Proc. SPIE*, 2006, vol. 5730, pp. 59–72.
[26] L. W. Snyman, M. du Plessis, and H. Aharoni, "Injection-avalanche based n+pn Si CMOS LED's (450 nm-750 nm) with two order increase in light emission intensity—Applications for next generation silicon-based optoelectronics," *Jpn. J. Appl. Phys.*, vol. 46, no. 4B, pp. 2474–2480, 2007.

[27] L. W. Snyman and M. du Plessis, "Increasing the emission intensity of p+np+ CMOS LED's (450–750 nm) by means of depletion layer profiling and reach-through techniques," in *Silicon Photonics III*, J. A. Kubby and G. T. Reed, Eds. Bellingham, W.A.: SPIE, May 2008, vol. 6898, Proc. SPIE.
[28] M. S. Tyagi, "Zener and avalanche breakdown in silicon alloyed p-n junctions," *Solid State Electron.*, vol. 11, pp. 577–582, 1968.
[29] S. M. Sze, *Semiconductor Devices, Physics and Technology*. Hoboken, NJ: Wiley, 1985, ch. 2.
[30] N. A. Drozdov, A. A. Patrin, and V. D. Tkachev, "Analysis of point defect and dislocation interaction in silicon on radiative spectra," *Sov. Phys. (JEPTP) Lett.*, vol. 23, p. 597, 1976.
[31] M. Reiche, K. Scheerschmidt, D. Conrad, R. Scholz, A. Plössl, U. Gösela, and K. N. Tu, "Dislocation engineering for LED light emission at 1.5 micron," *Inst. Phys. Conf. Ser.*, vol. 157, p. 447, 1997.
[32] M. A. Green, J. Zhao, A. Wang, P. J. Reece, and M. Gal, "Efficient silicon light emitting diodes," *Nature*, vol. 412, p. 805, 2001.
[33] M. Kittler, M. Reiche, T. Mchedlidze, T. Arguirov, G. Jia, W. Sifert, S. Suckov, and T. Wilhelm, "Stark effect at dislocations in silcon for modulation of a 1.5 μm light emitter," in *Silicon Photonics III*, J. A. Kubby and G. T. Reed, Eds. Bellingham, W.A.: SPIE, May 2008, vol. 6898, Proc. SPIE.
[34] Snyman *et al.*, 2008, unpublished research.
[35] J. C. Tsanga and J. A. Kash, "Pico-second hot electron light emission from submicron complementary metal-oxide-semiconductor circuits," *Appl. Phys. Lett.*, vol. 70, no. 7, pp. 889–891, Feb. 17, 1997.
[36] Austrian Mikro Systeme, 0,35 μm BiCMOS design and processing procedures Austrian Mikro Systeme, Graz, Austria.
[37] S. M. Sze, *Semiconductor Devices, Physics and Technology*. Hoboken, NJ: Wiley, 1985, ch. 4.
[38] L. W. Snyman, A. Bogalecki, L. M. Canning, M. du Plessis, and H. Aharoni, "High frequency optical integrated circuit design and first iteration realization in standard silicon CMOS integrated circuitry," in *Proc. 10th IEEE Int. Symp. Electron Devices and Opto-electronic Applications*, Manchester, U.K., Nov. 18–19, 2002, pp. 77–82.
[39] L. W. Snyman, L. M. Canning, A. Bogaleki, A. Aharoni, and M. du Plessis, "200-Mbps optical integrated circuit design and first iteration realizations in 0.8 micron bi-CMOS silicon integrated circuitry," in *Proc. SPIE* , vol. 5357-6, Optoelectronic Integration on Silicon II Conference at SPIE's Integrated Optoelectronic Devices 2004 Symposium as Part of Photonics West 2004.
[40] C. Janse van Rensburg and P. J. Venter, "High speed, low power CMOS optical receiver front-end," in *Proc. South Afr. Conf. on Semi and Superconducting Technol. (SACSST 2009)*, Cape Town, South Africa, Apr. 2009 [Online]. Available: http://research.ee.sun.ac.za/SACSST09

Lukas Willem Snyman (M'92) received the B.Sc., B.Sc Hons., M.Sc., and Ph.D. degrees, all in semiconductor physics, from the University of Port Elizabeth, South Africa, in 1974, 1975, 1978, and 1987, respectively.

During the period 1988 to 1999, he was with the Carl and Emily Fuchs Institute for Microelectronics, University of Pretoria. South Africa, as an Associate Professor. Since October of 2000, he has been a Professor at the Tshwane University of Technology, Pretoria, currently the largest technical university in South Africa. His research interest includes optoelectronic devices, analog CMOS IC design, and microwave and high-frequency electronics. He started his research in CMOS Si LEDs in 1992 when he was at the University of Pretoria. During 1996, he spent sabbatical research leave as a Guest Scientist with the Department of Applied Solid State Physics, Paul Scherrer Institute Zurich, Switzerland and also at the Laboratory for Nanostructure, Villigen, Switzerland. Here he performed research of multilayer AlGaAs structure for optoelectronic applications and also on silicon bipolar and CMOS light-emitting devices At the SPIE 2001-Photonic West Symposium in San Jose, CA, January 2000, he gave a 30-min overview invited paper, and he also served on the program committee for the SPIE 2001 Conference on " Silicon and Hybrid Opto-electronics" held in San José. During 2007 he interfaced with a group at Boston University, Boston, MA. He has given several guest lecturer on CMOS light-emitting device design in the U.S., Switzerland, Japan, and Finland. He is the main author of two U.S. patents and six South Africa patents on the topic of CMOS light-emitting devices. He has to date published about 90 scientific articles, mostly in international conference proceedings and scientific journals.

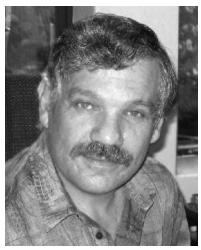

Monuko du Plessis (M'88–SM'00) received the B.Eng., M.Eng., and D.Eng. degrees in electrical and electronic engineering from the University of Pretoria, Pretoria, South Africa, in 1972, 1978, and 1984, respectively. He received the B.A degree in psychology and the B.Com. (Hons.) degree in economics from the University of South Africa, South Africa, in 1988 and 1998, respectively.

Since 1973, he has been with the Department of Electrical, Electronic and Computer Engineering, University of Pretoria, South Africa where he is director of the Carl and Emily Fuchs Institute for Microelectronics (CEFIM) since 1990. In 2008 he was named as one of the 100 Leading Minds of the University of Pretoria over the last 100 years, as part of the university centenary celebrations. His research interests include CMOS analog integrated circuit design, silicon photonics, and MEMS devices. He has published more than 170 research outputs in the form of scientific journal papers, conference proceedings, and patents.

Dr. du Plessis is the chapter chair of the IEEE in South Africa for the Electron Devices, Photonics, and Circuits and Systems societies. In 2004 he was appointed as an IEEE Electron Devices Distinguished Lecturer for IEEE Region 8. He is also the *Africa Research Journal* specialist editor for Electron Devices.

Enrico Bellotti received the Laurea in Ingegneria Electronica from the Politecnico di Milano, Milano, Italy, in 1989 and the Ph.D. degree in electrical engineering from the Georgia Institute of Technology, Atlanta, in 1999.

From September 2000 to August 2006, he held the position of Assistant Professor, and since September 2006 the position of Associate Professor with the Department of Electrical and Computer Engineering, Boston University, Boston, MA, where he is the leader of the Computational Electronics Group. His research activity focuses on the simulation of advanced semiconductor materials and electronics, optoelectronic, and photonics devices.

Prof. Bellotti was the recipient of the 2003 ONR Young Investigator Award and the 2005 NSF CAREER Award.